LUND UNIVERSITY
Faculty of Science

Many-body-based DFT treatment of fermions in optical lattices

Jérémie Westergren

Thesis submitted for the degree of Bachelor of Science
Project duration: 2 months, 15 hp

Supervised by Ass. Prof. Claudio Verdozzi and Miroslav Hopjan

LUND
UNIVERSITY

Department of Physics
Division of Mathematical Physics
May 2017

Abstract

With recent advances in the field of ultra cold atoms one can, by trapping atoms at low temperatures by laser beams, simulate systems which can be adequately described by single-band lattice Hamiltonians. Also, due to the high parameter tunability of the experimental setups, lattice disorder can be introduced in a controlled fashion in these systems. This thesis considers disordered/ordered interacting fermion lattice systems in equilibrium in one and two dimensions, subject to trapping parabolic potentials, where different levels of description, ranging from exact where possible (in 1D, Density Matrix Renormalization Group, DMRG), to approximate (based on several local-density approximations within the framework of Lattice Density Functional Theory) are used. The exchange-correlation potentials considered come from Many-Body Approximations obtained using Green's functions, as well as from an exact local-density approximation (LDA) based on the Bethe-Ansatz (BALDA) in 1D. Both one- and two-dimensional systems were studied in equilibrium, essentially looking at the ground state density profiles. Furthermore, in 2D, a pseudo-dynamics representing the trap-opening in the complete adiabatic limit was also studied. For one-dimensional systems, it is found that, in general, BALDA yields very good results compared to DMRG, except for the low density limit, but DMRG can describe features that none of the LDA:s considered can reproduce. It is also found that the strength of the external potential affects the impact that the exchange-correlation potential has on the system. Many of these features translate to the 2D case. However, a new aspect emerges in two dimensions, related to the competition of disorder and interaction. Here an important outcome is that, on opening the trap at an ideally adiabatic rate, different MBA:s (and thus different LDA:s) provide different minimal vs maximal expansion radii of the particle cloud, as a result of the interplay of disorder and interaction, and the underlying square lattice structure. For the 2D results, exact benchmarks were not available, and our findings may thus need further validation, by e.g. considering several disorder configurations or, ideally, by performing full Green's function calculations. These considerations are summarised in our conclusions and outlook remarks, where possible directions for future investigation are highlighted.

Acronyms

GS Ground State

DFT Density Functional Theory

KS Kohn-Sham

HK Hohenberg-Kohn

LDA Local Density Approximation

BALDA Bethe-Ansatz Local Density Approximation

MBA Many-Body Approximation

TMA T-Matrix

2B Second Born

GW Screened interaction

DMRG Density Matrix Renormalization Group

Contents

1 Introduction

Describing realistic quantum many-body systems is a daunting task that has troubled many physicists since the advent of quantum mechanics. The solution to this problem is of utmost importance if we want to understand the world around us, considering how practically all systems that have any relevance to humans are comprised of a very large numbers of particles (the Avogadro number, $N_A \approx 10^{24}$, is usually used to define the macroscopic limit). While quantum mechanics in principle gives the correct description of any (non-relativistic) system, most calculation involving a macroscopic number of particles is in practice impossible, in spite of the increase in computational power that has been achieved over the last few decades. In order to circumvent this obstacle, physicists need to find ways to obtain knowledge about the system at hand, without solving for the many-body wavefunction of the system. A case in point is Density Functional Theory [1, 2], which is the main topic of this thesis.

When faced with the task of simplifying a practically intractable problem to something that can actually be calculated, there is no single obviously correct approach. One must often rely on physical intuition in deciding how to reduce the problem to one that is tractable. One way to tackle this problem is to focus on certain aspects of the problem, and try to replace the Hamiltonian of the initial problem with a simpler model Hamiltonian [2], which still retains the properties of interest. One particular model Hamiltonian which is of great interest to the condensed matter community is the Hubbard model [3]. The Hubbard model is a lattice model, in which the position eigenstates are discretised. In its most simple incarnation, the particles can tunnel between nearest neighbour sites, like in the tight binding model, and interact locally with particles on the same site. Since its conception in the 1960s, the Hubbard model has been used to study phenomena such as magnetism, electron correlation and high temperature superconductors [4], but interest in this model has greatly increased recently because of its ability to accurately describe ultracold atoms in optical lattices.

The field of ultracold atoms [5] can be said to have had its genesis with the experimental observation of Bose-Einstein condensate in 1995 [6]. Development of techniques such as laser cooling, which began being developed as early as in the 1960s [7], also played a large role to its emergence [7]. The field have later on expanded to also include the treatment of fermions. Ultracold atoms can be trapped in optical lattices, consisting of counterpropagating lasers forming standing waves, resulting in a static landscape with evenly spaced lattice sites. By utilising the so called Feshbach-resonances [8, 7] one can emulate repulsive or attractive fermions(bosons) on a discrete lattice, such as described by the Hubbard model. The parameters of these systems, e.g. the strength of the on-site interaction, can be controlled with very good precision, and effects like disorder, which is an inseparable part of any real solid state system, can be introduced in a controlled fashion.

The close resemblance to ideal systems provides an optimal setting to study for example the interplay between interaction and disorder, which is one of the topics of this thesis. Furthermore, the field of ultracold atoms is a research area in which new theoretical approaches are needed in order to interpret experimental results [7]. On the theoretical side, much has already been done in 1D, see for example Refs. [9, 10], where exact numerical

methods such as DMRG are viable. In higher dimensions, much less is known at present, though higher dimensions remains an active area of research [11, 12].

Furthermore, by choosing the right formulation of the initial problem, solutions tend to not be as elusive as they may be within the generic wavefunction formulation of quantum mechanics. One formulation which is conceptually easy to grasp is Density Functional Theory (DFT), which is an exact reformulation of quantum mechanics where the particle density plays the main part, rather than the wave function from the Schrödinger formulation, or the state vectors in the matrix mechanics formulation. Calculations within DFT have the advantage of being computationally inexpensive, relative to other methods, which enables one to treat quite sizeable systems efficiently. The central quantity within the DFT formulation is the so-called exchange-correlation potential, which encompasses all the many-body intricacies of the system, and is defined as the variational derivative of the exchange-correlation energy with respect to the density. However, even though DFT is an exact reformulation of quantum mechanics, we must employ approximations in order to make use of the theory in practice. The exchange-correlation energy is usually the main object of approximation, and is taken from a reference system in which analytic, numerically exact, or reliable approximate solutions are accessible.

As an example of a reference system Fig. 1 displays the exchange-correlation potential obtained from a Hubbard dimer occupied by two repulsive fermions with interaction strength U. Note the symmetry around half-filling, which is a general feature exhibited by exchange-correlation potentials of fermionic systems on a bipartite lattice. The exchange-correlation potential of such a rudimentary system could in principle be applied to larger and more complex systems to obtain qualitative results, but in order to obtain quantitative results exchange-correlation potentials from more sophisticated reference systems are a necessity.

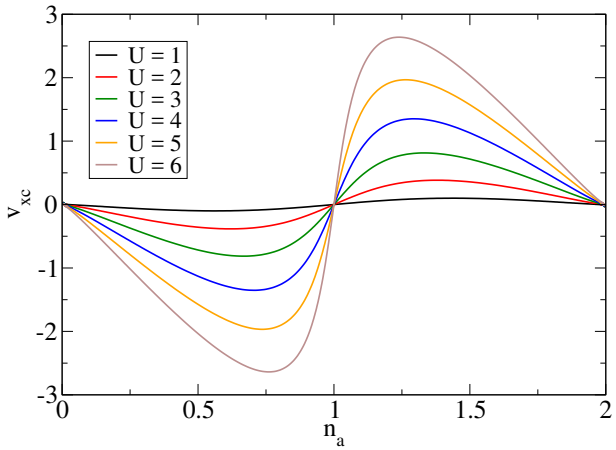

Figure 1: Exchange-correlation potential obtained from exact numerical solutions of a Hubbard dimer (a two-site system) occupied by two repulsive fermions of opposite spin, for 6 different interaction strengths U. The exchange-correlation potential, v_{xc}, is plotted against the density n. The subscript a refers to the site index, as the fixed number of particles enables a full description of the system by only studying one of the sites.

Another approach to the many-body problem is to try to approximate the solution by initially neglecting the many-body effects on the system, and include them later in a perturbative manner. In this approach, one-particle Green's functions can be used to

compute the expectation values of any one-particle operators, but also quantities like the total energy. The different approximation schemes for Green's functions can be visualised in terms of Feynman diagrams, which is of great aid when traversing into uncharted territory where physical intuition is the primary guiding light.

For systems with a small number of interacting particles, exact numerical diagonalization is also an option, but the size of the systems which can be treated by this approach is at present limited to 10-20 particles. A more sophisticated and powerful method of the exact kind is the Density Matrix Renormalization Group (DMRG). Solutions from these methods can be used as benchmarks against which the approximate solutions are evaluated. For a few, very simple systems, one may be inspired and find an analytical solution to the problem. The systems for which there are analytical solutions available are rare. The analytical expressions obtained from such systems may serve as a starting point from which analysis of more complex systems may be undertaken.

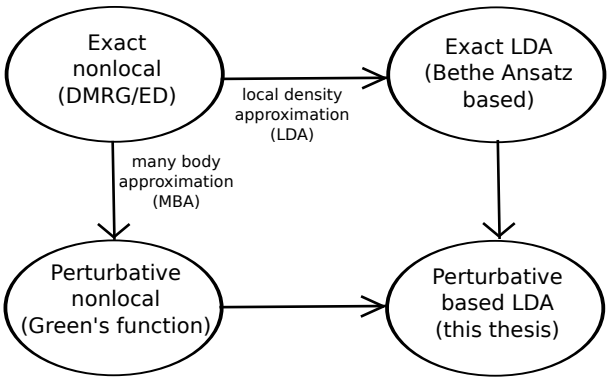

Figure 2: Pictorial description of the different levels of description for the systems under consideration. The primary focus of this thesis is on the bottom left MBA-based LDA.

The goal of this thesis is to compare different levels of description from various combinations of all above mentioned approaches, (see Fig. 2, where the different levels of description are displayed pictorially). The model chosen as the stage for this study is the 1D and 2D fermionic Hubbard model, where ground-state calculations will be undertaken. Both ordered and disordered systems will be considered, in an attempt to evaluate the effects of disorder on fermions in optical lattices. The primary view point will be that of DFT, used in an approximate fashion, with many-body approximations (MBA) entering as means to approximate the exchange-correlation potential of the reference system. In one dimension, exact DMRG calculations will be performed. The analytical solution to the Hubbard model based on the Bethe-ansatz, will be utilised to provide exchange-correlation potentials (BALDA) for DFT calculations. This provides benchmarks to which the approximate results stemming from the MBA potentials can be evaluated. This corresponds to the top left (DMRG), top right (BALDA) and bottom right (MBA-LDA) bubbles in Fig. 2, respectively. The conclusions from the calculations in 1D, where much is already known from earlier studies [10, 13, 14], will then be carried over to 2D, where much less is known and only MBA potentials are available, in order to provide some insight in the performance of the new approximate potentials.

2 Theory

2.1 Density functional theory

Density Functional Theory (DFT) has its origin in the 1964 Hohenberg-Kohn paper [1] (HK). HK proved that there is a unique mapping between the external potential and the ground-state one particle density, up to a constant in the potential. From this follows that also the groundstate (GS) wavefunction, Ψ_n, is uniquely determined by the GS-density, except for multiplication by an arbitrary phase. Utilising this correspondence, the universal functional,

$$F[n] \equiv \langle \Psi_n | \hat{T} + \hat{U} | \Psi_n \rangle \tag{1}$$

can be defined, where $\hat{T}$ and $\hat{U}$ are the kinetic and inter-particle interaction operators, respectively. From $F[n(r)]$, the energy functional is defined,

$$E_v[n] \equiv \int v(r)n(r)dr + F[n] \tag{2}$$

where $v(r)$ is the external potential. The need to define the energy functional as a Legendre transform of $F[n]$ arises from the fact that the density, n, is the variational derivative of the energy with respect to the external potential, and one cannot completely specify a function in terms of its derivative. HK subsequently proved that $E_v[n]$ is minimized for the correct GS-density. Thus the problem of determining the ground state properties of a system is exactly reformulated into a variational problem in the one particle density. However, due to the equivalence of the wavefunction and DFT descriptions, the complexity of the problem is unchanged. Obtaining $F[n]$ requires the same effort as solving the initial Schrödinger equation. In order to make use of DFT one must find means of approximating $F[n]$.

2.2 Kohn-Sham one particle scheme

In the previous section, DFT was presented as an alternative way of describing quantum mechanical systems, but without any suggestions for how DFT can be applied in practice. One way of approaching the problem of determining $F[n]$ is to employ a method where quantities that are easily calculated are extracted from the density functional, with the hopes that the remaining part will be small and can be treated approximately. Kohn and Sham [15] (KS) proposed a separation of $F[n]$ into three parts,

$$F[n] = T[n] + U[n] = T_0[n] + E_H[n] + E_{xc}[n] \tag{3}$$

where $T_0[n]$ is the non-interacting part of the kinetic energy, $E_H[n] = \frac{1}{2}\int\int \frac{n(r)n(r')drdr'}{|r-r'|}$ is the Hartree energy and $E_{xc}[n] = T_{xc}[n] + U_{xc}[n]$ is the contributions to the kinetic and interaction energy due to exchange and correlation between particles. KS introduced a fictitious non-interacting system, tailored to have the same density as the original system, from which $T_0[n]$ is obtained as the kinetic energy. The KS-equations have the form,

$$(-\frac{1}{2} \bigtriangledown^2 + v_{ks})\phi_i = \epsilon_i \phi_i \tag{4}$$

where ϕ_i are the KS-orbitals and v_{ks} is the KS-potential, defined as

$$v_{ks} = v_{ext} + \frac{\delta E_H}{\delta n} + \frac{\delta E_{xc}}{\delta n} = v_{ext} + v_H + v_{xc} \tag{5}$$

where $\frac{\delta}{\delta n}$ represents the variational derivative with respect to the density. As v_{ks} depends on the density, the set of equations (4) have be solved self-consistently. In general, the eigenvalues and the solutions to the KS-equation do not have any obvious physical interpretation. One exception is that the energy of the highest occupied KS-orbital corresponds to the ionization energy of the system [16]. Otherwise, the KS-orbitals can be seen as mathematical tools for obtaining the GS-density [2]. The density is obtained by squaring and summing up all the filled KS-orbitals,

$$n = \sum_{i,\sigma}^{occ} |\phi_{i\sigma}|^2 \tag{6}$$

where the index σ indicates summing over spins. The Hartree potential, $v_H = \int \frac{n(r')dr'}{|r-r'|}$, is explicitly known and the external potential, v_{ext}, is given. This leaves one with the problem of determining the exchange-correlation potential, v_{xc}, which contains all the exchange and correlation effects of the system. Solving self-consistent one particle equations is a relatively simple task, so once v_{xc} is known or adequately approximated, all the GS-properties of the system can be calculated. It is, however, not certain that arbitrary densities can be reproduced by a non-interacting KS-system, i.e. if it is *non-interacting v representable*. Looking at eq (5) one can see that representability is directly related to the existence of the variational derivative $\frac{\delta E_{xc}}{\delta n}$ [2].

However, the exchange-correlation potential is a highly complicated object, which depends non-locally on the density, and it is known only for a few very simple systems. Hence this is the point where approximations must be made in order to make progress in the KS-approach. One drastic simplification that can be made, is to assume that the exchange-correlation potential is not explicitly non-local, i.e. the exchange-correlation potential can be expressed as a regular function of the local density, $v_{xc}[n(r)] = v_{xc}(n)$, rather than a functional of the entire density profile. Such a *local density approximation* (LDA) is obtained by solving a reference system where the exchange-correlation potential has the aforementioned property of not being explicitly non-local. This reference system is solved exactly or approximately and from the obtained solution an exchange-correlation potential can be extracted. The far most common reference system for LDA is the free electron gas, or in the case of lattice DFT [17], the homogeneous Hubbard model. In this latter case, the exchange-correlation potential is obtained by taking the variational derivative of the exchange-correlation energy per site with respect to the density. We wish to note that, in a strict sense, the LDA is not a mean field method, since it includes electronic correlations [2].

2.3 Lattice DFT and the Hubbard model

While the original HK theorems dealt with a reformulation of quantum mechanics into a theory where the continuous one-particle density is the basic variable, one might ask if the framework of DFT can be used to reformulate problems in terms of some local variable other than the density. Schönhammer, Gunnarsson and Noack [18] studied the underlying

theoretical framework of DFT, where they extended the HK theorem pertaining to the minimization of the energy functional for the correct GS-density, to functionals of any local variable which couples linearly to an external parameter. One of these DFT type theories is *Site Occupation Functional Theory* (SOFT), introduced by Schönhammer and Gunnarsson [17] , which is a lattice DFT where the site occupation number assumes the role of the density type variable.

Lattice DFT has one obvious advantage over its continuous counterpart, which is that the standard reference system for obtaining the exchange-correlation potential, the Homogeneous Hubbard model, is analytically solvable in one dimension [9]. In contrast, the paradigm reference system for continuous DFT, the homogeneous electron gas, has no analytical solution [4].

The Hubbard model is a lattice model introduced first by John Hubbard in 1963 [3]. The model was developed in order to study correlation effects in transition and rare-earth metals where the electron gas description is no longer appropriate. For systems where the electron density is concentrated around the nuclei that make up the lattice, and the overlap of electrons orbiting different nuclei is small, it seems reasonable to adopt a lattice description where only the interaction of electrons located around the same nucleus is taken into account. In its most basic form, the Hamiltonian of the Hubbard model written in second quantization is,

$$\hat{H} = -t_{ij} \sum_{\langle i,j\rangle,\sigma} (\hat{c}^{\dagger}_{i,\sigma}\hat{c}_{j,\sigma} + \hat{c}^{\dagger}_{j,\sigma}\hat{c}_{i,\sigma}) + U \sum_{i} \hat{c}^{\dagger}_{i,\uparrow}\hat{c}_{i,\uparrow}\hat{c}^{\dagger}_{i,\downarrow}\hat{c}_{i,\downarrow} \tag{7}$$

where $\hat{c}^{\dagger}_{i,\sigma}, \hat{c}_{i,\sigma}$ are creation and annihilation operators for a fermion with spin σ at site i and $\hat{c}^{\dagger}_{i,\sigma}\hat{c}_{i,\sigma} = \hat{n}_{i,\sigma}$ is the spin resolved site occupation number operator. The hopping matrix, t_{ij}, controls the tunnelling rate between the sites i and j, and U is the on-site interaction. Each lattice site has a single energy level, and can accommodate one electron of each spin. The particular form of the Hamiltonian in equation (7) is valid for any dimensionality, and the geometry of the system is defined by the hopping matrix, t_{ij}. In the present work we consider only geometries where $t_{ij} = t = 1$ for nearest neighbours and $t_{ij} = 0$ otherwise, hence the subscripts will be dropped from here on. Note that all quantities in this thesis e.g. interaction U, external potential v_{ext} and disorder W are expressed in units of t. Thus the unit charge, e, and $\hbar$ are set to be equal to one.

To study the behaviour of electrons on a lattice subject to an external perturbation, an additional term must be added to the Hamiltonian in equation (7),

$$\hat{H} = -t \sum_{\langle i,j\rangle,\sigma} (\hat{c}^{\dagger}_{i,\sigma}\hat{c}_{j,\sigma} + \hat{c}^{\dagger}_{j,\sigma}\hat{c}_{i,\sigma}) + U \sum_{i=1} \hat{c}^{\dagger}_{i,\uparrow}\hat{c}_{i,\uparrow}\hat{c}^{\dagger}_{i,\downarrow}\hat{c}_{i,\downarrow} + \sum_{i,\sigma} \hat{n}_{i,\sigma} v_{i,\sigma} \tag{8}$$

where v_i is the external potential at site i. While equations (7) and (8) are spin resolved, only spin independent external potentials are considered in this thesis.

2.4 Self-consistent solutions of the Kohn-Sham equations

In order to obtain the GS-density using DFT, the corresponding Kohn-Sham one particle equations were solved, by means of exact diagonalization described in section 3.1,

$$(\hat{T} + \hat{v}_{ks})\phi_\mu = \epsilon_\mu \phi_\mu \tag{9}$$

where since $v_{ks}(n)$ is a function of the density itself, one must adopt a self-consistent iterative approach. This method consist of choosing an initial density $\{n_i\}$, usually the density of the corresponding non-interacting system, which is obtained by first solving the KS-equations for $v_{ks} = v_{ext}$. A new KS-potential is then assembled according to,

$$v_{ks}(i) = v_{ext}(i) + v_H(n_i) + v_{xc}(n_i) \tag{10}$$

where $v_H(n_i) = \frac{1}{2}Un_i^2$ is the Hartree-potential and the exchange-correlation potential v_{xc} is obtained from a homogeneous reference system, $v_{xc}(n) = v_{xc}^{ref}(n)$. This new KS-potential is then used to compute the density, and this is repeated until the difference between two consecutively computed densities is below some threshold value, i.e. convergence is reached. In order to avoid getting stuck in a self consistent loop, a mixing parameter α is introduced, and the new densities, $\{n'\}$, are obtained by linear mixing of the density from the previous step and the density calculated at the current step.

$$n'_{i,t+1} = \alpha n_{i,t+1} + (1-\alpha)n'_{i,t} \tag{11}$$

where t indicates the number of iterations. $1 > \alpha > 0$, usually with $\alpha \ll 1$.

3 Other Methods

3.1 Exact Diagonalization

In this thesis, exact diagonalization [4, 19], in the sense of arbitrary numerical precision, was used to solve the smallest systems under consideration. The DSYEV routine contained in LAPACK [20] was used to obtain the eigenvalues and eigenvectors of the Hamiltonian. Exact diagonalization quickly becomes intractable, considering that the dimensionality of the Hilbert space grows (considering only systems with fixed spin) as $\binom{L}{N_\uparrow}\binom{L}{N_\downarrow}$, where L is the number of lattice sites and N_σ is the number of fermions with spin σ. Diagonalizing the corresponding matrices quickly gets out of hand, considering that direct and full diagonalization of matrices grows in complexity as the cube of the dimensionality of the matrix.

3.2 Density Matrix Renormalization Group Calculations

DMRG was used to obtain numerically exact GS-densities in 1D. The DMRG algorithm for an infinite 1D chain is implemented as follows [21]:

1. A small subset of the system, called left block is coupled to a single neighbouring site, making an enlarged block.

2. The enlarged left block is then coupled to a similarly constructed enlarged right block, and the ground state for this system, called a super block, is found through exact diagonalization.

3. From the groundstate the reduced density matrix of the left enlarged block is constructed, and a truncated basis is defined from the eigenstates of the density matrix with the largest statistical weights.

4. All the relevant operators and the groundstate are then renormalized to the new truncated basis and the process is repeated until the desired system size is reached.

This process works for infinite systems (where the process would be repeated until e.g. the groundstate energy has converged), but to apply it to finite systems one has to modify the algorithm once the super block reaches the size of the finite system under consideration. At this point one starts to reduce the size of the right block as the left block grows. All the right blocks needed from this point on has already been constructed in previous steps, and the two sites joining the left and right block "sweep" across the chain until the end of the chain is reached. The role of the left and right blocks are then reversed, and the sweeping starts in the opposite direction. After each sweep a better approximation for the groundstate is found, and convergence is reached typically within a few sweeps [22, 21]. The point of this method is that, instead of just keeping the energetically lowest lying states of the iteratively growing left block, implicitly assuming that the ground state of the entire system can be described in terms of low energy states of the subsystems, one keep the statistically most favourable states of the left block coupled to the environment (the right block).

3.3 Methods for the infinite homogeneous Hubbard model

In the context of DFT, the 1D Hubbard model has the advantage that it is analytically solvable in the homogeneous case (as mentioned earlier in section 2.3) using Bethe-ansatz [9], which is not the case for the homogeneous electron gas. The exact solution allows one to construct an optimal LDA denoted BALDA, where the acronym stands for Bethe-Ansatz Local Density Approximation.

However, for the two-dimensional Hubbard model, the exact solution for the ground state energy is lacking, and the available numerically approximate solutions are inadequate around half-filling ($n = 1$) [11]. This prevents us from finding the exact (paramagnetic) ground state energies for an optimal LDA. Thus one has to resort to approximate solutions, which may work in certain parameter ranges. Here we choose to compute the ground state energies with the many-body diagrammatic method for computing the Green's functions [23]. That is, we work with the second Born approximation (2B), T-matrix approximation [24] (TMA) and GW approximation [25], and test their performance in relation to each other.

The approximations can be represented by self-consistently dressed diagrams, which respect certain conservation laws of Baym and Kadanoff [26]. For the dressed diagrams, the total energy can be computed with the so-called Galitskii-Migdal formula [27], which for the homogeneous system can be written in $(\omega, \mathbf{q})$ space [28]:

$$\begin{aligned} E_{tot.} &= \frac{-1}{(2\pi)^{D+1}} \int_{-\infty}^{\infty} \int_{BZ} d\omega d\mathbf{q} (\omega + \epsilon_{\mathbf{q}}) \mathrm{Im} G^R(\omega, \mathbf{q}) f(\omega) \\ n &= \frac{-2}{(2\pi)^{D+1}} \int_{-\infty}^{\infty} \int_{BZ} d\omega d\mathbf{q} \mathrm{Im} G^R(\omega, \mathbf{q}) f(\omega). \end{aligned} \tag{12}$$

with D being the dimensionality, G^R the retarded propagator [23], $\epsilon_{\mathbf{q}}$ the single particle energy and f the statistical Fermi factor. For the homogeneous Hubbard reference system, we use

$$v_{xc}^{appr.}(n) = \frac{\partial E_{xc}^{appr.}(n)}{\partial n} \tag{12}$$

where $E_{xc}^{appr.}(n) = E_{tot.}^{appr.}(n) - T_0(n) + E_H(n)$.[1] The three terms on the right hand side are the total energy in the particular approximation, the non-interacting kinetic energy and the Hartree energy for the D-dimensional homogeneous Hubbard model, respectively.

It is convenient to perform calculations in $(\omega, \mathbf{q})$ space. For example, for the 2B case, one gets:

$$\begin{aligned} G(\omega, \mathbf{q}) &= \frac{1}{\omega - \epsilon(\mathbf{q}) - v_H - \Sigma_{xc}^{2B}(\omega, \mathbf{q})}, \\ \Sigma_{xc}^{2B}(\omega, \mathbf{q}) &= \frac{U^2}{(2\pi)^{2(D+1)}} \int_{-\infty}^{\infty} \int_{-\infty}^{\infty} \int_{BZ} \int_{BZ} d\omega' d\omega'' d\mathbf{q}' d\mathbf{q}' \\ &\times G(\omega', \mathbf{q}') G(\omega'', \mathbf{q}'') G(\omega - \omega' + \omega'', \mathbf{q} - \mathbf{q}' + \mathbf{q}''), \end{aligned}$$

[1] The actual calculation of $E_{tot}^{appr.}(n)$ was outside the scope of this thesis, and details are deferred to a future publication, see J. Westergren, M. Hopjan and C. Verdozzi, in preparation.

where $G(\omega, \mathbf{q})$ is the time ordered propagator. The equations are iterated until self-consistency is reached.

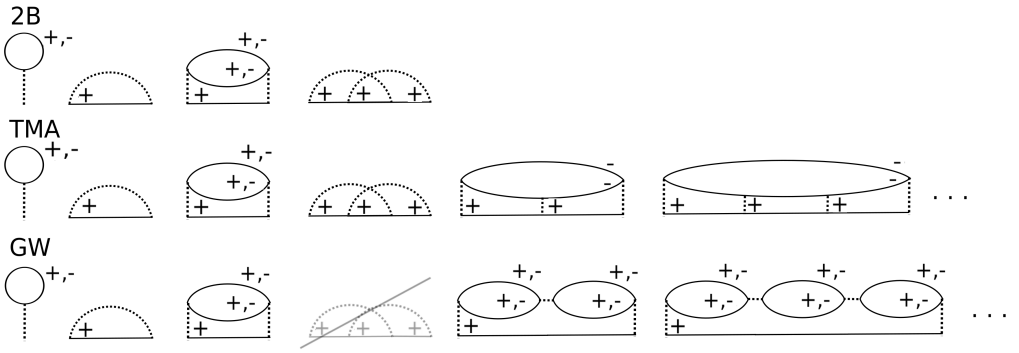

Figure 3: Diagrammatic representation of the many-body self-energies used in this thesis. The top row is the 2B approximation which includes all diagrams up to second order. The middle row is the TMA, which includes all the so called ladder diagrams up to infinite order. The GW approximation includes all bubble diagrams up to infinite order, which represents repeated electron-hole creation and annihilation. The + and − signs in the diagrams represent the different spin projections of the propagators.

Fig. 3 displays the diagrams for the chosen approximations. The 2B approximation contains all diagrams up to second order, thus it is not expected to work for strong interactions. The TMA and GW approximations include diagrams of a certain type up to infinite order. The TMA is suitable for low (high) filling and short range interactions (e.g. Hubbard interaction), where the diagrams describing multiple scattering events between the same two particles become the dominant contribution to the self-energy. One can show, that for the one-band fermionic Hubbard Hamiltonian, in the TMA approximation, the contribution from the exchange diagrams exactly cancel the contribution from same spin direct diagrams [29, 30]. Hence in the diagrammatic expansion in Fig. 3, beyond second order, this cancelation is already taken into account. The GW performs better for systems with long range weak interactions, where screening is caused by electron-hole excitations. Since the Hubbard model describes short range interactions, it is expected that TMA should perform well at low (high) filling.

4 Results

The results emerging from this study can be divided into three parts. Section 4.1 consists of an analysis of the exchange-correlation potentials from approximate and exact solutions for the homogeneous Hubbard model in one, two and three dimensions. The analysis is focused primarily on the behaviour of the potentials in the dilute limit ($n = 0 - 0.3$), and how well they perform in relation to the available exact potentials in one and three dimensions. The conclusions from the analysis of the potentials in one and three dimensions will then be carried over to 2D, in order to make an educated guess about the quality of the approximate potentials in 2D.

In section 4.2 the available exchange-correlation potentials in one dimension are used to perform DFT ground-state calculations of repulsive fermions in a Hubbard chain subject to an external parabolic potential, primarily for the low density limit. This serves to describe an important class of experiments where cold atoms in optical lattices are subjected to an external potential forcing the particles to the centre of the lattice. Both ordered and disordered cases are considered, and all the DFT calculations are compared to numerically exact benchmarks coming from DMRG calculations. This serves to provide insight into how accurately the LDA potentials from the homogeneous Hubbard model can describe the correlation effects in these non-homogeneous systems, and to investigate for which external parameters the LDA breaks down. The study in one dimension also seeks to highlight what effect the differences in the approximate and exact LDA potentials have on the density profile of the system. The conclusions from this part provides additional understanding of how capable the approximate LDA:s are in capturing the features of the true system, which are then utilized in the investigation of the two dimensional Hubbard model.

Section 4.3 deals with results from DFT ground-state calculations in the two dimensional Hubbard model, once again subject to an external parabolic trapping potential. As in 1D, both ordered and disordered systems are being treated, in order to try to disentangle the effects of interaction from those of disorder. To achieve that, the radii of the fermionic clouds are examined in the absence and presence of disorder. In 2D there is no numerically exact solution or exact LDA available, hence all the exchange-correlation potentials come from approximate perturbative solutions to the homogeneous Hubbard model. However, the conclusions from the first two parts provide a reasonably firm foundation for the analysis of the results, even in the absence of numerically exact or exact LDA benchmarks. Furthermore, dynamics in the fully adiabatic limit is emulated by performing ground-state calculations for varying strengths of the parabolic potential, which is to be understood as adiabatically removing the trapping potential for a system of ultracold atoms and letting them expand into an optical lattice.

4.1 Exchange-correlation potentials for the infinite homogeneous Hubbard model

In this section the exchange-correlation potentials from exact and approximate solutions to the infinite homogeneous Hubbard model (in one, two and three dimensions) are presented, and trends of the potentials with respect to dimensionality and level of approximation are discussed. However, in the subsequent sections, only 1D and 2D potentials are applied, and here the potentials from the solutions of the three dimensional Hubbard model are dis-

played in order to support our educated guess about the quality of the approximate potentials in two dimensions. In Fig. 4 the potentials for one, two and three dimensions, are displayed[2].

Starting the discussion with the 1D potentials, the approximate perturbative solutions are compared with the exact solution by Lieb and Wu [9]. The exact (non-perturbative) solution shows a discontinuity at half-filling, reflecting Mott physics which in 1D persists for all non-zero interaction strengths. None of the approximate solutions are able to reproduce the discontinuity at half-filling; this is a typical feature of the MBA solutions and can be seen already for the non-self-consistent second Born approximation, see [18, 33]. Another general feature of the approximate solutions, is that they approach zero for zero filling. Among the approximate solutions, TMA behaves better in comparison to the exact solution, at low and high filling (0-0.3 and 1.7-2.0), than 2B and GW; the latter two overestimate the exchange-correlation potential in this density range. Additionally, in the density range (0.3-0.5), despite the devation of TMA from the exact solution, the derivative of the TMA potential still maintains the same sign as the derivative of the exact potential. This is not the case for the 2B and GW potentials, which exhibit the complete opposite behaviour in this density range.

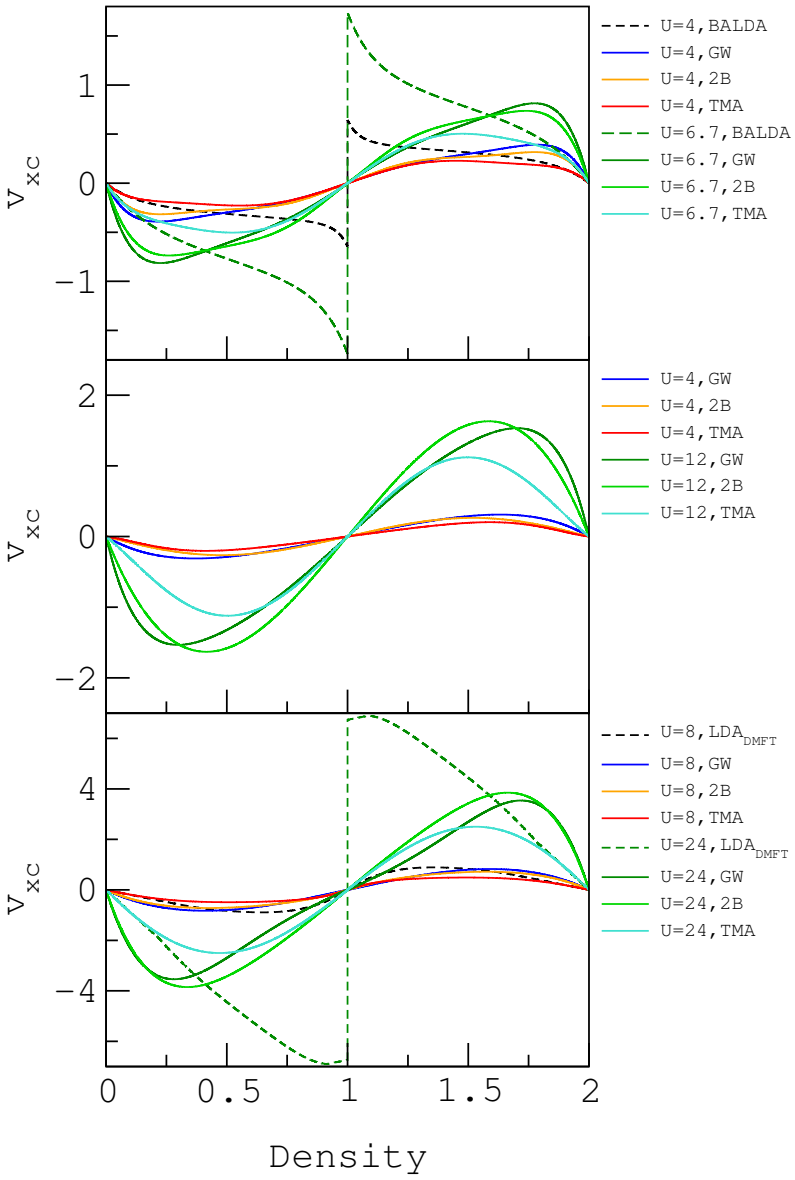

Figure 4: Exchange-correlation potential, v_{xc} for various values of U, as a function of the total density. Top is 1D, mid 2D and bottom 3D.

Next is the 3D Hubbard model where the "exact"[3] (paramagnetic) solution is obtained from Dynamical Mean Field Theory [34] (DMFT), where a 3D cubic lattice is mapped

[2]Some of the potentials in Fig. 4 are taken from previous works. In 1D the BALDA and 2B potentials were reported in [31], and the TMA for $U = 4$ is taken from [28]. In 3D the DMFT-LDA:s come from [32] while the 2B potentials as well as TMA for $U = 24$ are coming from [28]. All the other potentials, and in particular the 2D potentials have not previously been reported.

[3]Exact in limit of infinite dimension.

onto an Anderson impurity model [32]. Here the discontinuity occurs only above a critical interaction strength. The analysis of the perturbative potentials is similar to the 1D case. The TMA is generally superior in comparison to the 2B and GW approximations, and the TMA potential approaches the "exact" one for low and high filling (0-0.3 and 1.7-2.0). As for the one dimensional case the approximate solutions do not predict a discontinuity, for any interaction strength.

The similar conclusions emerging from the 1D and 3D potentials allow us to make an educated guess about the behaviour and quality of the approximation in 2D. In 2D the approximate solutions cannot be compared to exact solutions, however the relative behaviour of the approximate solutions, see Fig. 4, tells us that the potentials exhibit similar behaviour to the 1D and 3D case with respect to each other. There are no surprises in terms of behaviour at low (high) densities and at half-filling. Arguably one can make a bold statement, and say that: *In 2D it is again the TMA which is superior compared to the 2B and GW approximations.* This means that TMA gives approximately exact description of the potential at lower and higher filling (0-0.3 and 1.7-2.0). Justified by the conclusions on the behaviour of the approximate potentials in relation to the exact solution in 1D and 2D, as well as the observation that the hierarchy of the approximations is retained also in 2D, TMA will be used at lower fillings as a "close to exact" solution, and the performance of the other approximate potentials in relation to TMA will be elaborated on in the following sections.

We note that the used interaction strengths U were not chosen consistently in relation to the bandwidth, $W = 2zt$, where z is the number of nearest neighbours and t is the hopping parameter. In one dimension, the choice of $U = 4$ over $U = 2$ for the weaker interaction case was made to make features in the potentials and the corresponding density profiles more readily visible for discussion. This can be compared to the results in section 4.3 where, in 2D, for $U = 4$ there are hardly any differences in the density profiles coming from the three approximate LDA:s. The stronger interaction $U = 6.7$ was chosen as it was found to give the strongly correlated regime [28]. In 2D, there were no potentials available at the time this study was initiated, and the interactions $U = 4$ and $U = 12$ were chosen simply as two values symmetric around the bandwidth $W = 8$. In three dimensions, the interactions $U = 8$ and $U = 24$ were chosen as there were already DMFT results available for these interaction strengths from earlier works [32].

4.2 One dimensional fermionic systems in parabolic traps

In this section results from GS-calculations of a 1D Hubbard chain, with number of sites $L = 100$, are presented. The system is subject to an external parabolic potential $v_{ext} = k(i - L/2)^2$. The GS-densities were obtained using the KS-LDA-scheme described in section 3.2, with v_{xc} coming from the exact Bethe-Ansatz (BALDA) and MBA solutions to the reference system, the homogeneous 1D Hubbard model. Three different MBA:s were used, TMA, 2B and GW. The results from the GS-calculations were compared to exact DMRG benchmarks in order to get insight into where LDA:s based on the homogeneous Hubbard model are permissible.

It is important to note that we are dealing with 3 different levels of description here, see Fig. 2. In the LDA one approximates the exchange-correlation potential of the system of interest by the v_{xc} of the reference system. The BALDA is thus an exact LDA. The MBA potentials, TMA, 2B and GW, are obtained from further simplifications, where the reference system is only solved approximately. The agreement of DMRG and BALDA

shows that the effects of correlations are inherently local (however, one should keep in mind that v_{xc}^{BALDA} contains all non-local correlations of the homogeneous reference system). Furthermore, comparisons between the densities obtained from approximate LDA:s and BALDA are indicative of when the approximations capture the true behaviour of the reference system. This two-step comparison is necessary due to the two levels of approximation for v_{xc} from MBA:s. There might be systems where an MBA-LDA outperforms BALDA compared to DMRG by mere coincidence, due to the errors from the two levels of approximation cancelling.

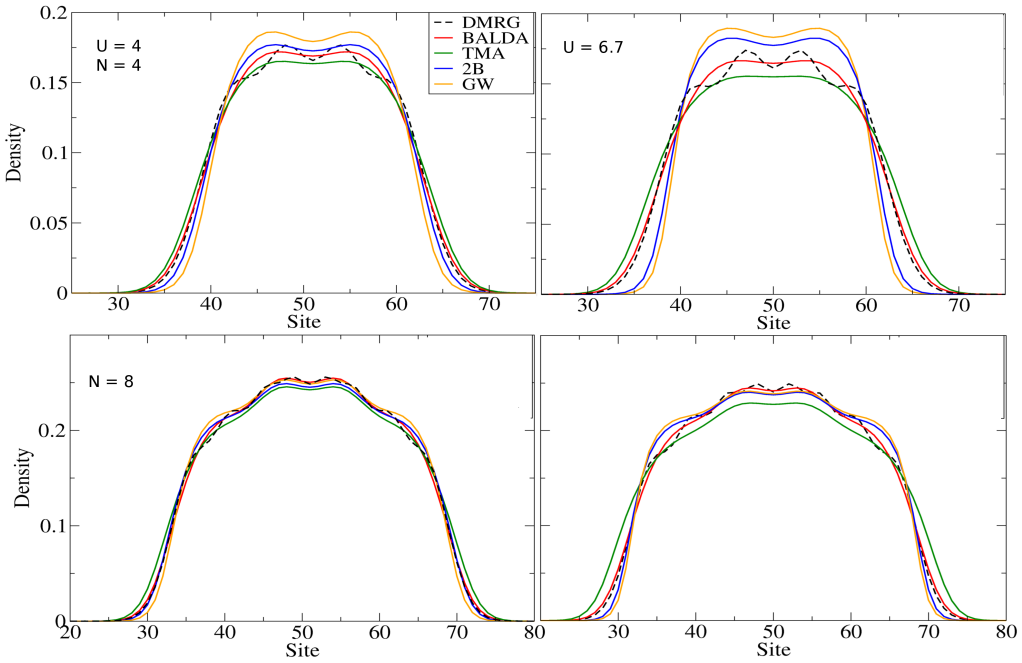

Figure 5: Comparison of BALDA and approximate LDA:s TMA, 2B and GW with DMRG. The densities are plotted against site number of a system consisting of $L = 100$ sites trapped in a parabolic potential with $k = 0.001$. Left panels corresponds to U = 4, Right panels to U = 6.7. Top panels corresponds to 4 fermions and bottom panels 8 fermions.

Fig. 5 displays results from calculations on systems with 4 and 8 repulsive fermions, on a $L = 100$ chain subject to an external potential $v_{ext}(i) = k(i - L/2)^2$ with $k = 0.001$. Calculations were made for U = 4 and U = 6.7. For these particle numbers the density is kept far away from half-filling, where the approximate LDA:s are expected to break down, due to the lack of a discontinuity in the exchange-correlation potential at half-filling [2]. The first thing one notices is that at the lowest particle number DMRG has features that none of the LDA:s are able to replicate, even though the BALDA solution follows the general shape of the exact solution. Moving up in particle numbers BALDA performs better and better and at 16 and 32 fermions it performs very well, for both U = 4 and U = 6.7, see Fig. 6. Note that even as the number of fermions are increased to 32, the system is still far away from half-filling. Out of the three approximate LDA:s, TMA does in general perform better than 2B and GW, as is expected from the analysis of the potentials in section 4.1, but also noted in a previous review [35]. For the densities where BALDA does well in comparison to DMRG, TMA is still off by a significant amount compared to BALDA. We also wish to remark that for all DFT calculations presented in this section, the density of the fermionic cloud is negligible at the boundaries (at most 10^{-5} at the boundary sites).

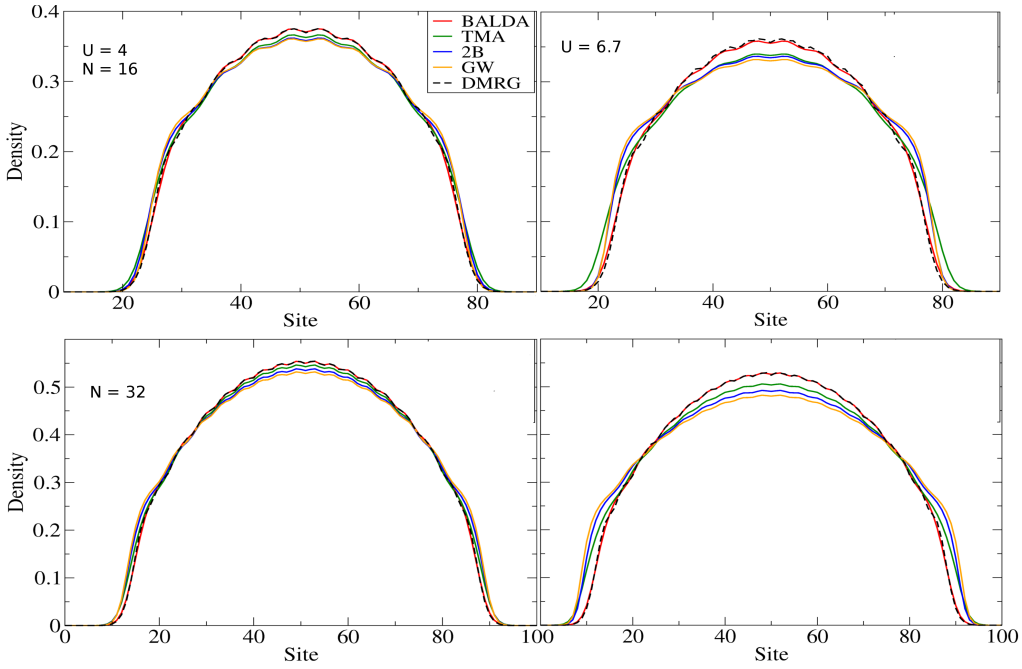

Figure 6: Densities plotted against site number of a system consisting of $L = 100$ sites trapped in a parabolic potential with $k = 0.001$. Top panels are 16 fermions and bottom panels 32 fermions. Left panels are U = 4, Right panels U = 6.7. Comparison of BALDA and approximate LDA:s TMA, 2B and GW with DMRG.

A closer inspection of 2B and GW results reveals that the density profiles for 4 particles are the narrowest, but becomes "squashed" as the particle number increases. Because of this GW and 2B happen to perform better at the top than TMA at 8 particles for both interaction strengths. To understand why this is happening one must look at the exchange-correlation potentials for GW and 2B, see Fig. 4. On speculative ground it appears that the nature of the density profile is affected by the steepness of the potential at low densities. For densities $n < 0.2$ the potential is decreasing, forcing particles to concentrate at the centre. At $n = 0.2$ there is a minimum, after which the potential increases. This has the effect of flattening the density profile. In between the narrow and flat density profiles, there is a "sweet-spot" where GW and 2B by coincidence just happen to perform better than TMA. Furthermore, at the lowest particle number the 2B and GW curves become more localized when going from weaker to stronger interaction, which goes against physical intuition. This behaviour was not observed for any of the other configurations in 1D.

The discrepancies between BALDA and DMRG at low density raises the question of why BALDA performs better as the density is increased. One possible explanation is that for the low density systems, the exchange-correlation potential plays a much larger role in shaping the density profile. This could lead to an exaggeration of features arising from small differences in the exchange-correlation potentials. Moving up in particle number, the interplay between the quickly increasing external potential in the boundary regions and the Hartree-Fock part of the on-site interactions takes control over shaping the density profile, resulting in a reduced impact of small differences in the exchange-correlation potentials. The features unique to the DMRG solution are present in all cases, but become less and less noticeable as the number of fermions are increased. Fig. 7 displays the density profiles arising from BALDA and Hartree-Fock given the density from BALDA, as well as the self-consistent HF-solution. The particle exchange is already taken into

account by the model itself. This means that HF, in practice, is the same as the Hartree approximation. The HF-solution obtained from the BALDA density is not self-consistent, but uses the BALDA density as a single input in order to obtain a HF-potential for which the single particle equations are solved for. This procedure seeks to highlight the impact the exchange-correlation potential will have on the system. As is readily visible, for 4 fermions, the non-self-consistent HF and BALDA have essentially nothing in common, while the density profiles at 32 fermions both have a large concentration of particles in the center of the parabola. This does seem to support the view that the properties of the system (i.e. the external potential and the number of fermions in it) dictates how big an impact the exchange-correlation potential has on the density.

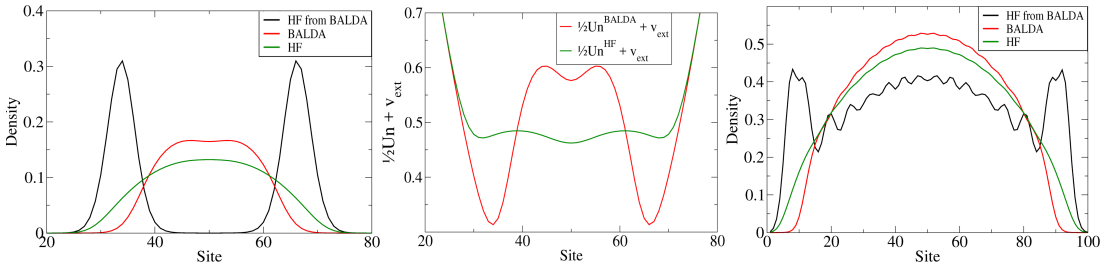

Figure 7: The density profiles from BALDA and a single Hartree-Fock calculation using the BALDA density to obtain the HF potential. The self-consistent BALDA and HF densities are also displayed for comparison. In all cases = 6.7. Left panel is for 4 fermions, right panel 32 fermions. The centre panel displays the HF plus external potential coming from the self-consistent BALDA and HF densities in the 4 fermion case.

Fig. 8 displays results from calculations of 70 repulsive fermions in an external parabolic potential with $k = 0.006$, for interaction strengths U = 4 and U = 6.7. Here the density in the centre goes well beyond 1, and it is clear that the approximate LDA:s cannot reproduce the plateau at $n = 1$. This region of constant density is called a Mott plateau and represents an insulating phase, brought on by the inter-particle interactions, as opposed to a band insulating phase arising from filled bands [13]. BALDA overestimates the features of the Mott-region compared to DMRG, which is most noticeable at $U = 4$, and predicts sharper edges of the transition. This can be compared to the results presented in a paper by G. Xianlong et al. [10] where BALDA was found to predict the existence of a Mott phase where numerically exact Quantum Monte Carlo calculations did not. The reason why the approximate LDA:s are unable to predict this phase transition can be attributed to the absence of a discontinuity in their corresponding v_{xc} at half-filling [2].

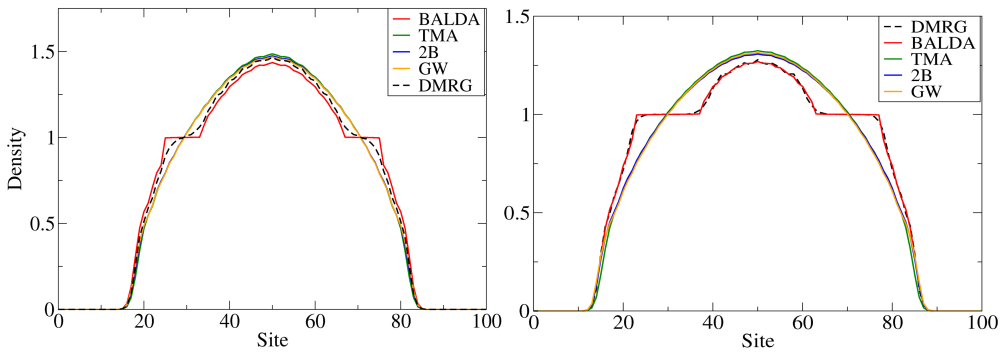

Figure 8: Comparison of BALDA and approximate LDA:s (TMA, 2B and GW) densities with DMRG. Left panels are U = 4, Right panels U = 6.7. The density is plotted against site number for a system consisting of $L = 100$ sites trapped in a parabolic potential with $k = 0.006$ for 70 fermions.

We finally briefly address the disordered case. Disorder was introduced into the 1D chain by letting $v_{ext,i} \rightarrow v_{ext,i} + W_i$, where W_i is selected from a uniform distribution between $W/2$ and $-W/2$, with $W = 0.5$ determining the strength of the disorder. Compared to the hopping parameter $t = 1$ this is considered to be fairly weak disorder. These are preliminary calculations that explore disorder only superficially. The calculations were made for only one set $\{W_i\}$. In the case of 32 fermions, it appears that the relative differences between the densities coming from the different potentials and DMRG are preserved for both $U = 4$ and $U = 6.7$, see Fig. 9. For the low density case, with only 4 fermions, the density from DMRG differs much more from the densities resulting from DFT calculations, while the differences between the MBA:s and BALDA are less pronounced, see Fig. 10. For 4 fermions, the differences between $U = 4$ and $U = 6.7$ for DMRG are hardly noticeable in the presence of disorder. Looking back at Fig. 5, we can see that this also seems to be the case in the absence of disorder. At present, we are unable to give a completely satisfactory explanation for this.

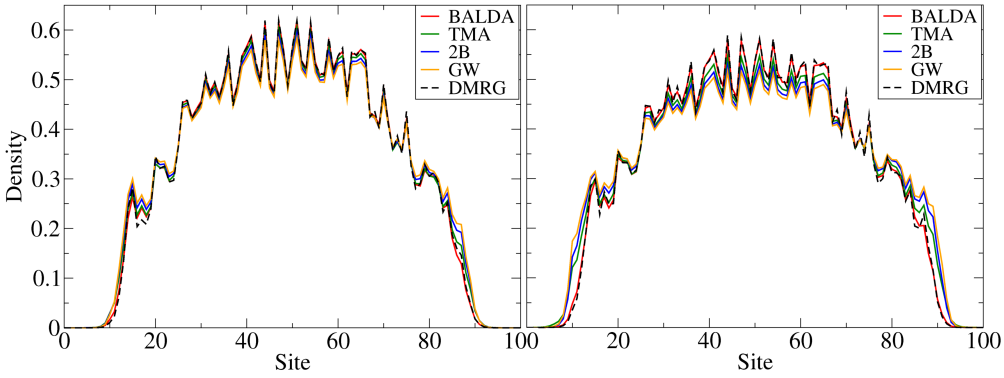

Figure 9: Comparison of BALDA and approximate LDA:s (TMA, 2B and GW) densities with DMRG in the presence of disorder $W = 0.5$. Left panels are U = 4, Right panels U = 6.7. The density is plotted against site number for a system consisting of $L = 100$ sites trapped in a parabolic potential with $k = 0.001$ for 32 fermions.

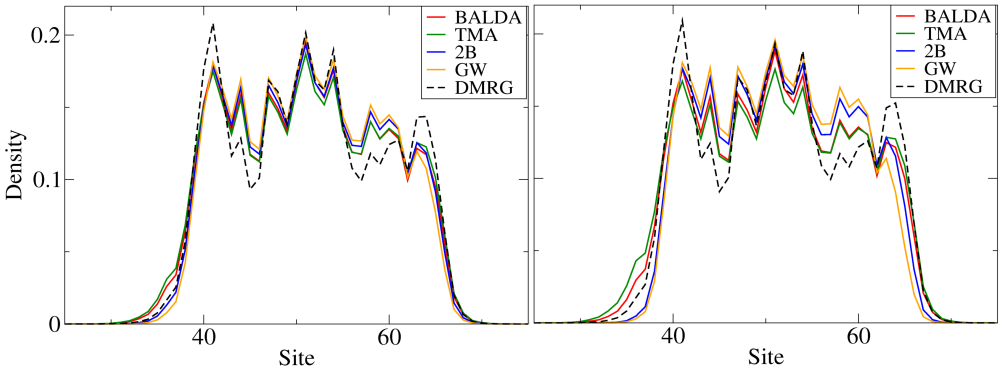

Figure 10: Comparison of BALDA and approximate LDA:s (TMA, 2B and GW) densities with DMRG in the presence of disorder $W = 0.5$. Left panels are U = 4, Right panels U = 6.7. The density is plotted against site number for a system consisting of $L = 100$ sites trapped in a parabolic potential with $k = 0.001$ for 4 fermions.

4.3 Two dimensional fermionic systems in parabolic traps

In this section we present DFT results for a 2D Hubbard lattice, obtained with an LDA based on TMA, 2B and GW. The lattice is once again exposed to an external parabolic potential $v_{ext}(i,j;k) = k((i-L/2)^2 + (j-L/2)^2)$. Calculations were made for two interaction strengths, $U = 4$ and $U = 12$. As opposed to the 1D case, there are no longer any exact, or exact LDA, benchmarks to compare to. The GS-densities were obtained by using the same Kohn-Sham method as in the 1D case. Due to the degeneracy arising from the symmetries of the 2D lattice and the circularly symmetric external potential, reaching convergence is sometimes very difficult. In the non-interacting case the KS-eigenstates can be grouped into shells like a harmonic oscillator, where the degeneracy of the states inside the shells is lifted due to the absence of perfect rotational symmetry. But as the interaction strength increases, some degeneracies seem to become resolved while new degeneracies emerge, making it very hard to find particle numbers for which the calculations converge for all 3 potentials. Eventually, this was possible for a number of cases, those actually reported here.

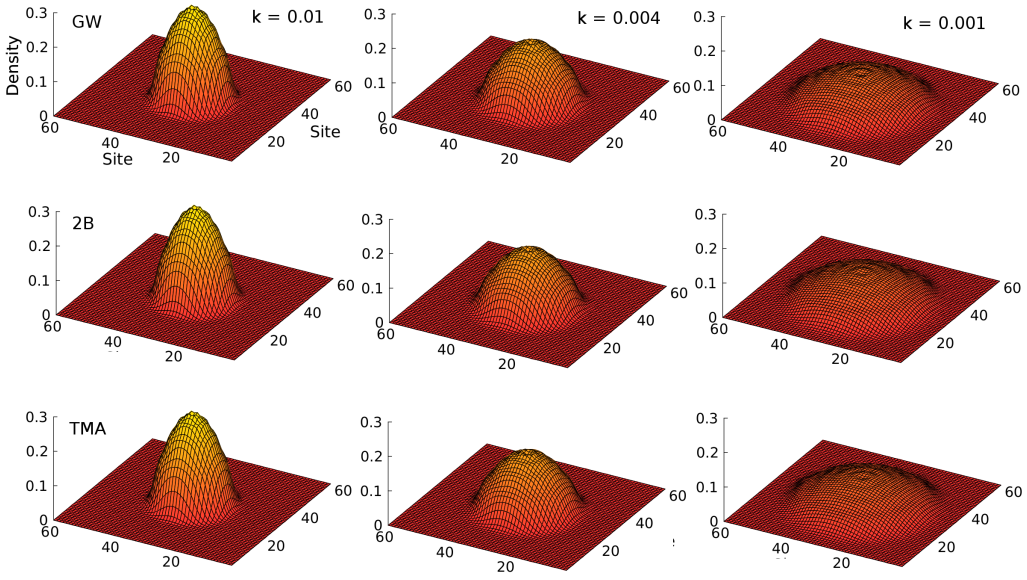

Figure 11: Density profile of 72 fermions on a 60 by 60 lattice, with interaction $U = 4$, from the three approximate LDA:s based on GW, 2B and TMA, in an external parabolic potential $v_{ext} = v(i,j;k)$ at 3 different strengths. Left column: $k = 0.01$, mid: $k = 0.004$ right: $k = 0.001$. Top panels are GW, mid panels are 2B and bottom panels are TMA results, respectively

To investigate the effects of disorder in the 2D Hubbard model, disorder of the form $v_{ext,i} \to v_{ext,i} + W_i$, where W_i is selected from a uniform distribution between $W/2$ and $-W/2$, with $W = 1$ determining the strength of the disorder. The set $\{W_i\}$ was chosen to be the same for all calculations. Note that this means that only one disordered setup is considered in these calculations. We plan to systematically investigate the role of several disorder configurations in a follow-up work. Here, within an exploratory perspective, we focus only on one disorder configuration. Calculations were performed on a system consisting of 72 repulsive fermion, for three different strengths of the external potential, $k = 10^{-2}$, $k = 4 \times 10^{-3}$, $k = 10^{-3}$, in order to emulate dynamics in the fully adiabatic limit. As in the previous section, the fermionic cloud never touches the boundary in any of the presented results.

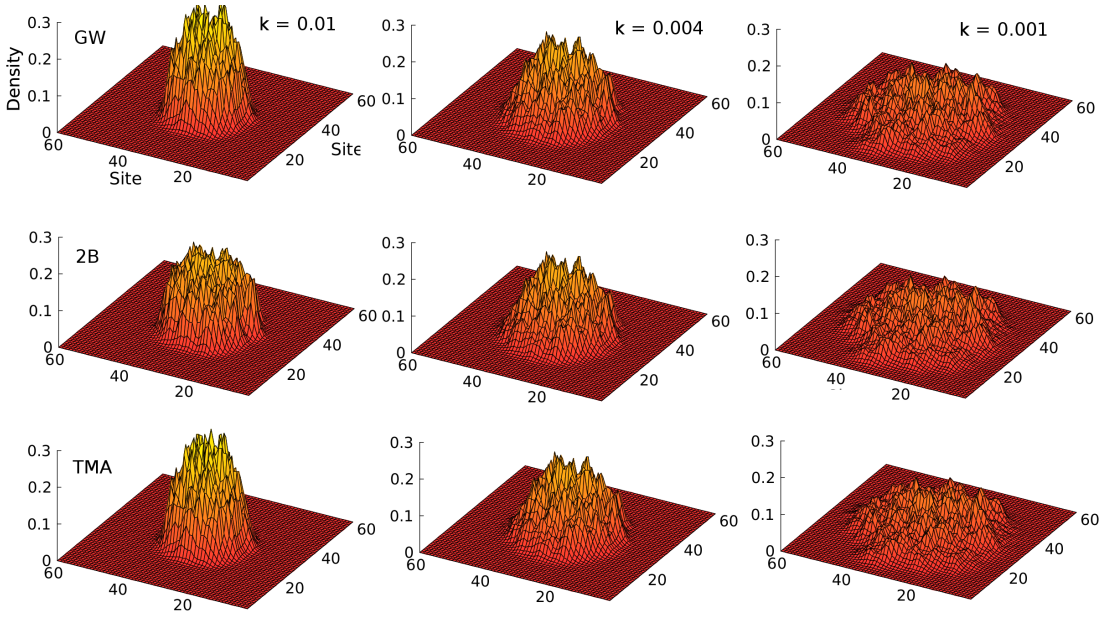

Figure 12: Density profile of 72 fermions on a 60 by 60 lattice, with interaction $U = 4$, in the presence of disorder $W = 1$, from the three approximate LDA:s based on GW, 2B and TMA, in an external parabolic potential $v_{ext} = v(i, j; k)$ at 3 different strengths. Left column: $k = 0.01$, mid: $k = 0.004$ right: $k = 0.001$. Top panels are GW, mid panels are 2B and bottom panels are TMA results, respectively

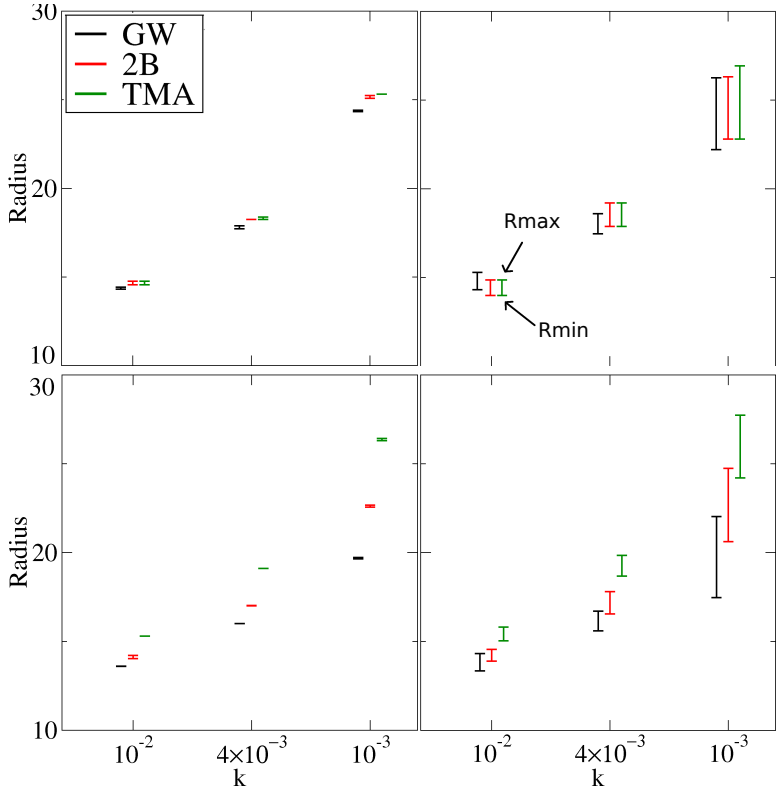

Figure 13: Maximum and minimum radii at which the density of the fermionic cloud drops below 10^{-3}, for 72 fermions, for approximate LDA:s from GW, 2B and TMA, subject to parabolic potentials with 3 different strengths k. Top (bottom) of the bars are maximum (minimum) radius centred at the mean radius. Left panels are for the ordered case, and right panels are in the presence of disorder $W = 1$. Top panels are for $U = 4$ and bottom panels are for $U = 12$.

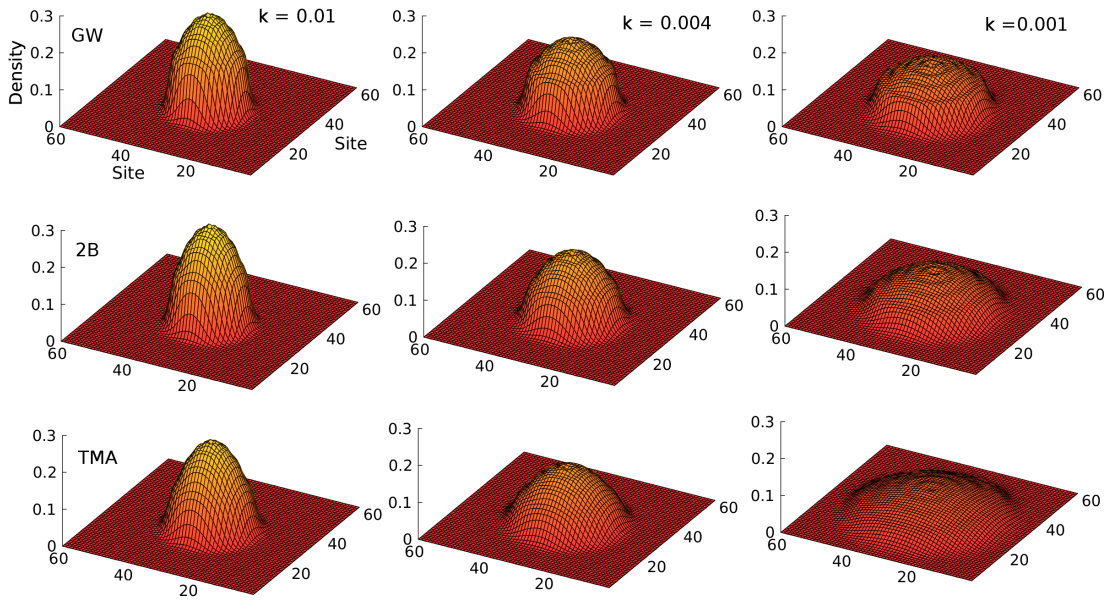

Figure 14: Density profile of 72 fermions on a 60 by 60 lattice, with interaction $U = 12$, from the three approximate LDA:s based on GW, 2B and TMA, in an external parabolic potential $v_{ext} = v(i, j; k)$ at 3 different strengths. Left column: $k = 0.01$, mid: $k = 0.004$ right: $k = 0.001$. Top panels are GW, mid panels are 2B and bottom panels are TMA results, respectively

What is apparent from looking at Fig. 11 is that for the weaker interaction strength, the density profiles arising from the three potentials are nearly identical. In Fig. 13 the radii at which the density of the clouds drops below 10^{-3} are plotted, which can be seen to reinforce the previous statement of the similarities between the density profiles at $U = 4$. Only GW yields a slightly more localized cloud compared to the others. The similarities between the 3 different approximate LDA:s persist in the presence of disorder, which only serves do destroy the nearly perfect circular symmetry which is observed in the ordered case. Upon increasing the interaction strength, the three potentials produce radically different results, with 2B and in particular GW being very resistant against expanding out into the lattice, see Fig. 14. Both 2B and GW are visibly more dense at the core for $U = 12$ compared to $U = 4$, which is counter-intuitive to how one would expect the system to behave upon increasing the interaction strength. However, this type of behaviour is hinted at already in section 4.2. This behaviour also persists under the influence of disorder.

To understand why this is happening, it is helpful to take a closer look at the exchange-correlation potential displayed in Fig. 4. The 2B and GW potentials for $U = 12$ are very steep in the low density regime. This can be compared to the discontinuity in the BALDA and DMFT potentials at half filling for 1D and 3D, which gives rise to the Mott insulating phase characterized by a region of uniform density [13, 12]. In particular the density profile arising from GW exhibits a similar behaviour, with a flatter top followed by a rapid decline in density at the edges of the cloud. Looking at Fig. 13, the significantly more localized behaviour of 2B and GW is clearly visible. For all three external potentials, 2B and GW becomes more localized upon increasing the interaction strength, while only TMA exhibits a tendency to delocalize when the interaction strength increases. Also for $U = 12$ the fermionic clouds exhibit nearly perfect circular symmetry in the ordered case.

As indicated from the results in 1D, the effects of the exchange-correlation potential on the density profile may vary significantly from system to system. This may serve as an additional explanation for the behaviour observed when the parabola is opened up. Looking at Fig. 14 and 13, for the weakest parabola $k = 0.001$ in the ordered system, the density from 2B differs more from GW than one might expect from simply looking at the differences in the exchange-correlation potentials. The differences in v_{xc} for 2B and GW are certainly smaller for this density range compared to the wider density range observed for the stronger external potentials, yet the difference in the density is far more pronounced. In the cases where the difference is most readily visible, see the leftmost panels in Fig. 14, all the exchange-correlation potentials are monotonically decreasing functions of the density, see Fig. 4, i.e. they all favour pushing the fermions to higher densities. This causes sort of an "avalanche" effect where higher densities favour increasing the density further. This amplifies the seemingly small differences between the potentials from 2B and GW, resulting in the different density profiles.

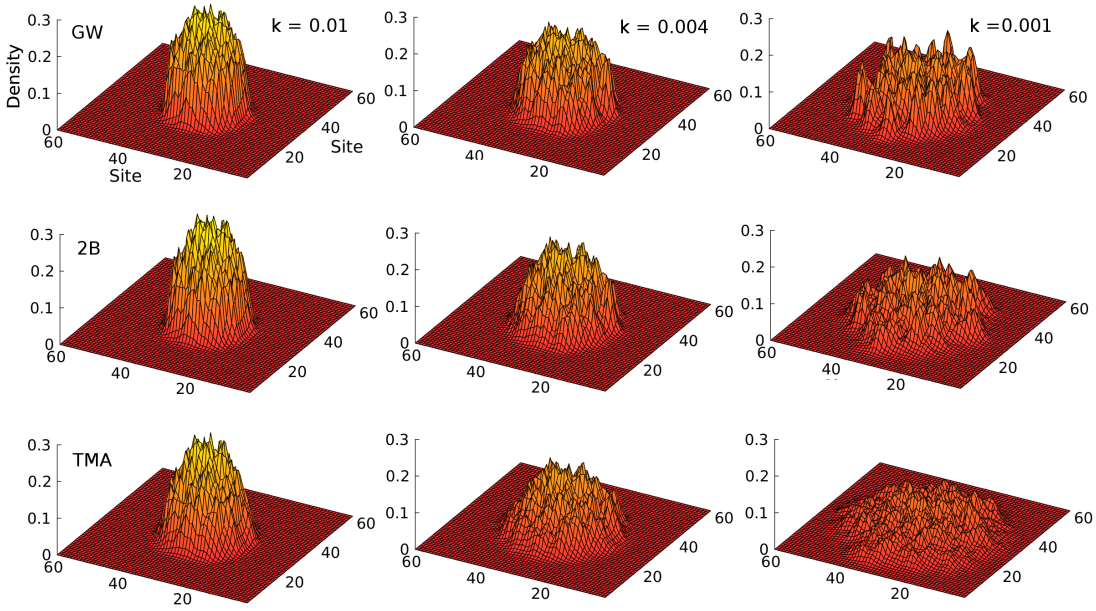

Figure 15: Density profile of 72 fermions on a 60 by 60 lattice, with interaction $U = 12$, in the presence of disorder $W = 1$, from the three approximate LDA:s based on GW, 2B and TMA, in an external parabolic potential $v_{ext} = v(i, j; k)$ at 3 different strengths. Left column: $k = 0.01$, mid: $k = 0.004$ right: $k = 0.001$. Top panels are GW, mid panels are 2B and bottom panels are TMA results, respectively

Note also how the difference that emerges between the maximum and minimum radii of the clouds, in the disordered case, when the interaction strength is increased. This can be seen by comparing the top right and bottom right panels in Fig. 13, where one can see that difference between maximum and minimum radius increases for GW and 2B, while it decreases for TMA, upon increasing U. This might just be an effect of the clouds covering different regions of the disordered lattice, in the cases where $U = 12$ (see bottom right panel in Fig. 13). However, another possible interpretation is that the interplay between interaction and disorder produces different results for TMA compared to GW and 2B, causing TMA to yield a more circularly symmetric cloud. Note again that these conclusions stem from calculations on only one disorder configuration, and are going to be re-examined for a large number of configurations in the future.

5 Conclusions and outlook

In this thesis, we have proposed and compared different levels of description (from exact to approximate) of ultracold fermion atoms in one and two dimensional optical lattices. The results from various approximations were mutually compared to highlight their similarities and differences. For 1D lattices, it was also possible to test the approximate treatments against numerically exact methods such as DMRG.

The primary accomplishment of this work has been the retrieval of exchange-correlation potentials for the 2D Hubbard model, and the determination of the TMA approximation as close to exact in the dilute limit.

A general feature emerging from our study is that the way differences in the exchange-correlation potentials reflects into differences of the corresponding densities is a non-trivial, system-dependent trait. That is, naive assessments of the potentials might not be enough to determine if the densities coming from different potentials are going to agree or not.

We also found that in one dimension, where DMRG and the exact LDA from the Bethe-ansatz are available, the TMA generally outperforms 2B and GW. Also, for the setups considered, TMA seems to be consistent relative to BALDA. On the other hand, the way 2B and GW density profiles compare to DMRG ones changes quite substantially upon varying parameters such as particle number or the external potential. Sometimes, in both one and two dimension, GW and 2B produced results which go against physical intuition: Namely, for some setups the density profile becomes more localized upon increasing the interaction strength, a behaviour not observed for TMA in any of the considered systems.

Regarding the interplay of interaction and disorder in 2D, our results hint that TMA might behave differently from 2B and GW, as e.g. it appears from the values of expansion radii at different strengths of the trapping potential. However, these indications are in no way conclusive, since only one disorder configuration was considered. In this case, the appropriate strategy would be to consider several disorder configurations, looking at averaged quantities or, better, at histogram distributions of the observable of interest (e.g. the expansion radii).

These last considerations make here a suitable place to restate that most of the work done in this thesis is quite exploratory in character, and in many aspects, rather incomplete. For example, as just said, our investigation and discussion of disorder only grasps the surface of the complex issue of how interactions and disorder mutually screen each other. In fact, as shown e.g. in the context of theories of many-body localization in disordered systems, an important role is played by temperature [36, 37]. A possible extension of the present work could be the inclusion of finite temperature effects within thermal DFT. Another methodologically interesting aspect to address is how exchange-correlation potentials from MBA:s evolve for hypercubic lattices of increasingly high dimensions, by e.g. determining the infinite dimensional limit of such potentials. A completely different and wide avenue for further progress would be to perform time-dependent adiabatic calculations with our DFT potentials. Studies of this sort would have a high degree of novelty for 2D systems and, as mentioned for the equilibrium case, they would permit to see how the behaviour of the cloud radii reported here would be modified in the presence of a truly dynamical (albeit adiabatic) opening of the confining potential.

These are some of the possibilities that come to mind at this stage to extend and generalize the work done in this thesis, and we look very much forward to the possibility of pursuing these (and other possible) lines of investigation in the future.

References

[1] P. Hohenberg and W. Kohn. Inhomogeneous electron gas. *Physical Review*, 136(3B):864–865, 1964.

[2] K. Capelle and V. L. Campo Jr. Density functionals and model Hamiltonians: pillars of many-particle physics. *Physics Reports*, 528:91–159, 2013.

[3] J. Hubbard. Electron correlations in narrow energy bands. *Proceedings of the Royal Society of London*, 276(1365):238–257, 1963.

[4] D. Karlsson. *Analytical and Numerical Developments in Strongly Correlated Systems: Perspectives from TDDFT and Green's Functions*. PhD thesis, 2014.

[5] I. Bloch. Ultracold quantum gases in optical lattices. *Nature Physics*, 1:23–30, 2005.

[6] M. H. Anderson, J. R. Ensher, M. R. Matthews, C. E. Wieman, and E. A. Cornell. Observation of Bose-Einstein condensation in a dilute atomic vapor. *Science*, 269:198–201, 1995.

[7] A. Kartsev. *Non-equilibrium fermions within lattice density functional theory: quantum transport and ultracold-atom phenomena*. PhD thesis, 2013.

[8] H. Feshbach. A unified theory for nuclear reactions. II. *Annals of physics*, 19:287–313, 1962.

[9] E. H. Lieb and F. Y. Wu. Absence of Mott transition in an exact solution of the short-range, one-band model in one dimension. *Physical Review Letters*, 20(25):1445–1448, 1968.

[10] G. Xianlong, M. P. Tosi M. Polini, V. L. Campo Jr., K. Capelle, and M. Rigol. Bethe-ansatz density-functional theory of ultracold repulsive fermions in one-dimensional optical lattices. *Physical Review B*, 73(165120), 2006.

[11] J. P. F. LeBlanc, Andrey E. Antipov, Federico Becca, Ireneusz W. Bulik, Garnet Kin-Lic Chan, Chia-Min Chung, Youjin Deng, Michel Ferrero, Thomas M. Henderson, Carlos A. Jiménez-Hoyos, E. Kozik, Xuan-Wen Liu, Andrew J. Millis, N. V. Prokof'ev, Mingpu Qin, Gustavo E. Scuseria, Hao Shi, B. V. Svistunov, Luca F. Tocchio, I. S. Tupitsyn, Steven R. White, Shiwei Zhang, Bo-Xiao Zheng, Zhenyue Zhu, and Emanuel Gull. Solutions of the two-dimensional Hubbard model: Benchmarks and results from a wide range of numerical algorithms. *Phys. Rev. X*, 5:041041, Dec 2015.

[12] A. Kartsev, D. Karlsson, A. Privitera, and C. Verdozzi. Three-dimensional dynamics of a fermionic Mott wedding-cake in clean and disordered optical lattices. *Scientific Reports*, 3(2570), 2013.

[13] D. Karlsson, C. Verdozzi, M. M. Odashima, and K. Capelle. Dynamical self-stabilization of the Mott insulator: Time evolution of the density and entanglement entropy of out-of-equilibrium cold fermion gases. *Europhysics Letters*, 93(2), 2011.

[14] G. Xianlong, M. Polini, M. P. Tosi, and B. Tanatar. Effects of disorder on the interacing Fermi gases in a one-dimensional optical lattice. *International Journal of Modern Physics B*, 2013.

[15] W. Kohn and L. J. Sham. Self-consistent equations including exchange and correlation effects. *Physical Review*, 140(4A):1133–1138, 1965.

[16] C.-O. Almbladh and U. von Barth. Exact results for the charge and spin densities, exchange correlation potentials, and density-functional eigenvalues. *Physical Review B*, 31:3231–3245, 1985.

[17] K. Schönhammer and O. Gunnarsson. Density-functional treatment of an exactly solvable semiconductor models. *Physical Review Letters*, 56(18):1068–1071, 1986.

[18] K. Schönhammer, O. Gunnarsson, and R.M Noack. Density-functional theory on a lattice: Comparison with exact numerical results for a model with strongly interacting correlated electrons. *Physical Review B*, 52(4):2504–2509, 1995.

[19] C. Verdozzi. Exact diagonalization studies of strongly correlated clusters, lecture notes for the doctorate programme in materials science, University of Milano-Bicocca, Italy, 2005.

[20] LAPACK — Linear Algebra PACKage, 2017.

[21] Gabriele De Chiara, Matteo Rizzi, Davide Rossini, and Simone Montangero. Density matrix renormalization group for dummies. *Journal of Computational and Theoretical Nanoscience*, 5(7), 2009.

[22] U. Schollwöck. The density-matrix renormalization group. *Reviews of Modern Physics*, 77, 2005.

[23] E.N Economou. *Green's Functions in Quantum Physics*. Springer, 3 edition, 2006.

[24] V.M. Galitskii. The energy spectrum of a non-ideal Fermi gas. *Sov. Phys. JETP*, 7(1):104, 1958.

[25] Lars Hedin. New method for calculating the one-particle Green's function with application to the electron-gas problem. *Phys. Rev.*, 139:A796–A823, Aug 1965.

[26] Gordon Baym and Leo P. Kadanoff. Conservation laws and correlation functions. *Phys. Rev.*, 124:287–299, Oct 1961.

[27] V.M. Galitskii and A.B. Migdal. Application of quantum field theory methods to the many body problem. *Sov. Phys. JETP*, 7(1):96, 1958.

[28] M. Hopjan, D. Karlsson, S. Ydman, C. Verdozzi, and C.-O. Almbladh. Merging features from Green's functions and time dependent density functional theory: A route to the description of correlated materials out of equilibrium? *Phys. Rev. Lett.*, 116:236402, Jun 2016.

[29] C. Verdozzi, P. J. Durham, R. J. Cole, and P. Weightman. Correlation and disorder effects in photoelectron and auger spectra: The late transition metals and their alloys. *Physical Review B.*, 55(24):16143–16158, 1997.

[30] M. Puig von Friesen, C. Verdozzi, and C.-O. Almbladh. Kadanoff-Baym dynamics of Hubbard clusters: Performance of many-body schemes, correlation-induced damping and multiple steady and quasi-steady states. *Physical Review B*, 82(155108), 2010.

[31] E. Boström, M. Hopjan, A. Kartsev, C. Verdozzi, and C.-O. Almbladh. Nonequilibrium green's functions and atom-surface dynamics: Simple views from a simple model system. *Journal of Physics: Conference Series*, 696(1):012007, 2016.

[32] Daniel Karlsson, Antonio Privitera, and Claudio Verdozzi. Time-Dependent Density-Functional Theory Meets Dynamical Mean-Field Theory: Real-Time Dynamics for the 3D Hubbard Model. *Phys. Rev. Lett.*, 106:116401, Mar 2011.

[33] Walter Metzner and Dieter Vollhardt. Ground-state energy of the D=1,2,3 dimensional Hubbard model in the weak-coupling limit. *Phys. Rev. B*, 39:4462–4466, Mar 1989.

[34] W. Metzner and D. Vollhardt. Correlated lattice fermions in D = ∞ dimensions. *Phys. Rev. Lett.*, 62:324–327, Jan 1989.

[35] C. Verdozzi, D. Karlsson, M. Puig von Friesen, C.-O. Almbladh, and U. von Barth. Some open questions in TDDFT: Clues from lattice models and Kadanoff–Baym dynamics. *Chemical Physics*, 391:37–49, 2011.

[36] Arijeet Pal and David A. Huse. Many-body localization phase transition. *Phys. Rev. B*, 82:174411, Nov 2010.

[37] Soumya Bera, Henning Schomerus, Fabian Heidrich-Meisner, and Jens H. Bardarson. Many-body localization characterized from a one-particle perspective. *Phys. Rev. Lett.*, 115:046603, Jul 2015.